Energy Engineering

Tech Science Press

https://doi.org/10.32604/ee.2026.069025

ARTICLE

Economic Optimization of Wind Solar Energy Storage Microgrid in the Northwest Gobi Region of China Based on Improved MDA Algorithm

Qingguo Nie and Yongfang Nie*

Nanchang Institute of Technology, Nanchang, China

*Corresponding Author: Yongfang Nie. Email: yongfangnie@163.com

Received: 12 June 2025; Accepted: 18 December 2025; Published: 27 May 2026

ABSTRACT: This study proposes an optimized design method for wind-solar-storage microgrid systems in the Gobi Desert region of northwest China. The core innovation is the development of a Modified Dragonfly Algorithm (MDA) to address the challenges of optimal system sizing and operation under complex desert conditions characterized by high renewable volatility and demanding environmental constraints. To strengthen the algorithm's global search capability and convergence speed, three key enhancements are introduced: optimal point set initialization for even population distribution, cosine similarity guidance for balanced exploration-exploitation, and a nonlinear convergence factor for adaptive adjustment. The multi-objective optimization model is evaluated using a comprehensive set of technical, economic, and environmental metrics. Simulation results for a case study demonstrate the effectiveness of the proposed approach. The optimized microgrid configuration achieves a total net present cost of 40.062 million CNY, a competitive levelized cost of energy of 0.452 CNY/kWh, and a high renewable energy penetration rate of 88.73%. Environmentally, the system significantly reduces carbon dioxide emissions by approximately 1403.35 t annually compared to conventional power supply. A detailed sensitivity analysis reveals that energy storage capacity, local wind speed variability, and load fluctuations are the most critical factors influencing system economy and operational stability. Furthermore, a financial feasibility assessment yields a positive net present value of 9.237 million CNY and an investment payback period of approximately 8.7 years. These results collectively confirm the proposed MDA-optimized microgrid design offers strong economic viability, technical reliability, and substantial environmental benefits for sustainable development in arid and remote desert regions.

KEYWORDS: Wind solar energy storage microgrid; dragonfly optimization algorithm; life cycle cost; penetration rate of renewable energy; financial analysis

1 Introduction

As the global energy structure accelerates towards low-carbon transformation, wind solar energy storage microgrids, as an important carrier for integrating renewable energy, have shown significant advantages in energy supply in remote areas [1]. The Gobi Desert region in northwest China, with its abundant solar and wind energy resources, has become an ideal area for developing off grid microgrids. However, the complex climate conditions, highly volatile load demands, and high proportion of renewable energy grid integration in the region pose technical challenges, making the economic optimization of microgrids a key issue that urgently needs to be addressed. How to reduce the full lifecycle cost of the system and improve the penetration rate of renewable energy while ensuring power supply reliability is the core proposition of current research [2,3]. To this end, the author focuses on the optimization configuration problem of wind solar energy storage microgrids in the Gobi region and proposes a multi-objective collaborative optimization method

based on an improved dragonfly optimization algorithm (MDA), aiming to provide theoretical support and practical path for energy system design in high-altitude and arid regions.

In the field of planning and optimization of wind solar energy storage microgrids, existing research has made certain progress. Zhu et al. proposed a location and capacity determination strategy for off grid wind solar energy storage charging stations based on path requirements, and optimized resource allocation efficiency through dynamic load forecasting. However, their research did not fully consider the coupling relationship between the cycle life and economy of the energy storage system [4]. Xu et al. explored capacity optimization configuration methods for distributed photovoltaic energy storage systems, with a focus on analyzing the matching mechanism between photovoltaic output and load fluctuations. However, their model has limited ability to handle multi energy collaborative scheduling and complex constraints [5]. Li et al. studied the capacity planning problem of water wind solar storage hybrid systems under high-dimensional uncertainty conditions. The introduction of probabilistic scenario generation technology improved the robustness of the system, but the algorithm convergence speed was slow and difficult to adapt to large-scale optimization requirements [6]. Wang et al. proposed an optimization method for rural microgrid wind power access architecture based on internal search algorithm, which achieved a balance between cost and reliability through multi-objective trade-offs. However, their research did not delve into the impact of algorithm initialization strategy on global optimization capability [7]. The above research provides useful references for modeling wind solar energy storage systems and designing multi-objective optimization algorithms, but there are still some shortcomings. Firstly, existing algorithms are prone to falling into local optima when solving high-dimensional and strongly constrained microgrid optimization problems, and the convergence efficiency urgently needs to be improved; Secondly, the dynamic coupling mechanism between the full lifecycle cost of energy storage systems and the volatility of renewable energy has not been fully quantified; The third issue is the insufficient construction of adaptive models for special environmental conditions in the Gobi region, such as dust attenuation and large temperature differences between day and night, which limits the engineering applicability of optimization results [8,9].

The core issues facing the economic optimization of wind solar energy storage microgrids can be summarized into three aspects. Firstly, traditional optimization algorithms suffer from low computational efficiency and unstable solution set quality when dealing with multi-objective and nonlinear constraint problems, making it difficult to meet the real-time scheduling requirements of complex microgrid systems [10]. Secondly, existing research mostly focuses on single energy types or static load scenarios, and there is insufficient collaborative modeling of the complementarity of wind and solar power output, seasonal fluctuations in load, and dynamic attenuation of energy storage, resulting in biases in the assessment of the full lifecycle cost of the system [11,12]. Thirdly, in response to the impact of extreme environments such as strong sandstorms and low temperatures on equipment performance in the Gobi region, existing models lack refined characterization, such as the dynamic characteristics of dust attenuation factors in photovoltaic modules that vary with seasons, and the constraints of wind turbine spacing on wind field efficiency. These factors significantly affect system economy and reliability, but have not been fully considered in most studies. In addition, there is a lack of research on hierarchical optimization strategies for microgrid energy management architecture in existing literature, which fails to effectively coordinate the contradiction between long-term planning and real-time scheduling, limiting further improvement of overall system performance [13,14].

In response to the above issues, the author proposes an economic optimization framework for wind solar energy storage microgrids based on an improved dragonfly optimization algorithm (MDA). Firstly, at the algorithmic level, a good point set initialization strategy is introduced to generate a uniformly distributed initial population through low difference sequences, enhancing global search capabilities; Combining cosine

similarity to dynamically adjust individual update direction and improve local optimization efficiency; Design a nonlinear convergence factor regulation mechanism to balance the weight allocation between algorithm exploration and development stages, effectively overcoming the shortcomings of traditional algorithms that are prone to premature convergence [15]. Secondly, at the system modeling level, a multidimensional refined model is constructed that includes wind speed height correction, dynamic factors of photovoltaic dust attenuation, and energy storage cycle life loss, accurately depicting the impact of environmental characteristics in the Gobi region on equipment performance. At the same time, a layered energy management architecture is designed to organically combine the capacity planning of the strategic layer, the day ahead scheduling of the tactical layer and the real-time control of the executive layer to realize the collaborative optimization of multiple time scales. Finally, by integrating net present value analysis, levelized electricity cost assessment, and carbon emission quantification models, a multi-objective optimization system covering economics, environment, and reliability is established [16]. This scheme can not only significantly improve the penetration rate and operational economy of renewable energy in microgrids, but also provide a universal methodological reference for optimizing energy systems in similar regions. Key findings show the improved MDA reduces convergence iterations by 21.6% and achieves 93.7% renewable penetration. The optimized system (1620 kW PV, 450 kW wind, 765 kWh storage) yields an LCOE of ¥0.452/kWh with 8.7-year payback. Compared to NSGA-II and WOA, the proposed improved MDA achieves faster convergence and more robust performance due to the integration of cosine similarity-based directional updates and a non-linear convergence factor. This enables efficient handling of high-dimensional optimization problems specific to Gobi microgrids.

2 Methods and Models

2.1 System Architecture and Modeling

(1) Wind power generation system model

The output power of wind turbines has a non-linear relationship with wind speed. When the wind speed is lower than the cut in wind speed or higher than the cut out wind speed, the wind turbine does not generate electrical energy; When the wind speed is between the cut in wind speed and the rated wind speed, the output power increases with the increase of wind speed; When the wind speed is between the rated wind speed and the cut-off wind speed, the fan operates stably at rated power [17]. The key technical parameters of the wind power generation system used in this study are presented in Table S1. The mathematical model of wind turbine output power adopted by the author is shown in Formula (1):

$$P_{wt}(v) = \begin{cases} 0, & v < v_{ci} or v > v_{co} \\ a \cdot v^3 - b \cdot P_r, & v_{ci} \le v < v_r \\ P_r, & v_r \le v \le v_{co} \end{cases} \quad (1)$$

In the formula, $P_{wt}(v)$ represents the output power of the wind turbine at wind speed v (kW); v_{ci} is the cutting wind speed (m/s); v_r is the rated wind speed (m/s); v_{co} is the cutting wind speed (m/s); P_r is the rated power of the fan (kW); a and b are power curve coefficients, which can be calculated by the following Formulas (2) and (3):

$$a = \frac{P_r}{v_r^3 - v_{ci}^3} \tag{2}$$

$$b = \frac{v_{ci}^3}{v_r^3 - v_{ci}^3} \tag{3}$$

The key parameters of the wind turbine used in this study are shown in Table 1.

Table 1: Architecture design of microgrid energy management system.

Architecture Level	Function Description	Time Scale	Key Algorithms/Models
Strategic layer	Capacity planning and long-term scheduling strategy	Month/Year	Improve MDA algorithm
Tactical layer	Pre/intra day optimization scheduling	Hour/day	Rolling Time Domain Optimization Strategy
Execution Layer	Real time power balance and control	Second/minute	Rule based rapid control

Due to the differences in wind speed at different heights in the Gobi region, it is necessary to correct the wind speed data measured at different heights [18]. The author uses exponential law to calculate the wind speed at the hub height, as shown in Formula (4):

$$v_h = v_r \cdot \left(\frac{h}{h_r}\right)^{\alpha} \tag{4}$$

Among them, v_h is the wind speed at the hub height h (m/s); v_r is the measured wind speed at reference height h_r (m/s); α is the surface roughness index, taken as 0.14 in the Gobi region. This wind speed height correction method can significantly improve the accuracy of wind power generation system models, especially in complex terrain Gobi regions [19].

(2) Photovoltaic power generation system model

The output power calculation model of the photovoltaic system is shown in Formula (5):

$$P_{pv} = P_{pv,STC} \cdot \frac{G_t}{G_{STC}} \cdot [1 + k_t \cdot (T_c - T_{STC})] \tag{5}$$

In the formula, P_{pv} is the actual output power of the photovoltaic system (kW); $P_{pv,STC}$ is the rated power of the photovoltaic system under standard testing conditions (kW); G_t is the actual solar radiation intensity received by the photovoltaic surface at the current time (W/m^2); G_{STC} is the radiation intensity under standard testing conditions, usually taken as 1000 W/m^2; k_t is the temperature correction coefficient, usually $-0.0045°C^{-1}$; T_c is the current operating temperature of the photovoltaic cell (°C); T_{STC} is the temperature under standard testing conditions, usually set at 25°C.

The operating temperature of photovoltaic cells can be calculated using the following equation, as shown in Formula (6):

$$T_c = T_a + \frac{NOCT - 20}{800} \cdot G_t \tag{6}$$

Among them, T_a is the ambient temperature (°C); *NOCT* is the nominal operating battery temperature (°C), typically between 42°C–48°C. The main parameters of the photovoltaic system used in this study are shown in Table S2.

For photovoltaic systems in the Gobi region, the impact of dust and sand accumulation on photovoltaic modules also needs to be considered [20]. The author introduces the dust attenuation factor (δ dust), and the revised photovoltaic output power is shown in Formula (7):

$$P_{pv,actual} = P_{pv} \cdot \delta_{dust} \cdot \eta_{inv} \tag{7}$$

Among them, η_{inv} is the inverter efficiency. The dust attenuation factor in the Gobi region varies seasonally, ranging from 0.85–0.90 in spring, 0.92–0.95 in summer, 0.90–0.92 in autumn, and 0.88–0.90 in winter.

Finally, the annual power generation of the photovoltaic system can be calculated using the following Formula (8):

$$E_{pv,year} = \sum_{t=1}^{8760} P_{pv,actual}(t) \cdot \Delta t \tag{8}$$

In the formula, Δt is the time step, usually taken as 1 h. Through this model, it is possible to accurately simulate the power generation behavior of photovoltaic systems in the Gobi region for 8760 h throughout the year.

(3) Battery Energy Storage System Model (BESS)

Constructing the charging and discharging behavior of a battery energy storage system using a dynamic state of charge (SOC) model. The SOC state update equation of the energy storage system is (9):

$$SOC(t+1) = \begin{cases} SOC(t) \cdot (1-\sigma) + \frac{P_{ch}(t) \cdot \eta_{ch} \cdot \Delta t}{E_{bess}}, & charge \\ SOC(t) \cdot (1-\sigma) - \frac{P_{dch}(t) \cdot \Delta t}{\eta_{dch} \cdot E_{bess}}, & discharge \end{cases} \tag{9}$$

In the formula, $SOC(t)$ and $SOC(t)$ represent the battery state of charge at time t and time t+1, respectively; σ is the self discharge rate of the battery; $P_{ch}(t)$ is the charging power (kW); $P_{dch}(t)$ is the discharge power (kW); η_{ch} and η_{dch} are the charging and discharging efficiencies, respectively; E_{bess} is the rated capacity of the battery energy storage system (kWh); Δt is the time step (h).

In order to protect the battery and extend its service life, the SOC of the battery needs to meet the following constraints as shown in Formulas (10)–(12):

$$SOC_{\min} \le SOC(t) \le SOC_{\max} \tag{10}$$

$$0 \le P_{ch}(t) \le P_{ch,\max} \tag{11}$$

$$0 \le P_{dch}(t) \le P_{dch,\max} \tag{12}$$

The main parameters of the battery energy storage system used in this study are shown in Table S3:

The life assessment of batteries is based on the nonlinear relationship between the depth of cycle (DOD) and the number of cycles, and the equivalent number of cycles of the battery can be calculated by rainflow counting method [21]. The calculation of battery lifecycle cost is shown in Formula (13):

$$C_{bess,lifecycle} = C_{bess,initial} \cdot \left[\frac{N_{eq}}{N_{rated}} \right] \tag{13}$$

Among them, $C_{bess,initial}$ is the initial investment cost of the battery; N_{eq} is the equivalent number of cycles; N_{rated} is the rated cycle life; $\lceil \rceil$ represents rounding up.

(4) Microgrid energy management architecture

The microgrid energy management architecture consists of three levels: strategic level, tactical level, and execution level, as shown in Table 1:

The core function of an energy management system is to coordinate the operation of various power generation units and energy storage systems, so that the system meets real-time power balance conditions as shown in Formula (14):

$$P_{pv}(t) + P_{wt}(t) + P_{dch}(t) - P_{ch}(t) + P_{dg}(t) = P_{load}(t) + P_{dump}(t) \tag{14}$$

In the formula, $P_{pv}(t)$ and $P_{wt}(t)$ represent the output power of photovoltaic and wind power, respectively; $P_{dch}(t)$ and $P_{ch}(t)$ represents the discharge and charging power of the battery, respectively; $P_{dg}(t)$ is the output power of the diesel generator; $P_{load}(t)$ is the load demand power; $P_{dump}(t)$ is the abandoned power.

The operation logic of the energy management system adopts a priority scheduling strategy, prioritizing the use of renewable energy, followed by energy storage systems, and finally using diesel generators as backup power sources [22]. The specific scheduling logic is as follows:

When renewable energy generation exceeds load demand:

a. Excess electricity is prioritized for battery charging

b. If the battery is fully charged or the charging power is limited, discard the battery

c. When renewable energy generation is less than the load demand:

d. Priority should be given to supplementing the power gap through battery discharge

e. If the battery SOC reaches the lower limit or the discharge power is insufficient, start the diesel generator

This operating logic can be optimized through the following cost function, as shown in Formula (15):

$$\min J = \sum_{t=1}^{T} \left[C_{pv}P_{pv}(t) + C_{wt}P_{wt}(t) + C_{bess}\left(P_{ch}(t), P_{dch}(t)\right) + C_{dg}P_{dg}(t) + C_{dump}P_{dump}(t) \right] \tag{15}$$

Among them, C_{pv}, C_{wt}, C_{bess}, C_{dg}, and C_{dump} are the unit operating costs of each part.

(5) Load and load model design

The load model adopted by the author is based on a typical daily electricity curve to fit the annual load demand, and introduces seasonal adjustment factors. The load power calculation Formula (16) is as follows:

$$P_{load}(t) = P_{base}(t) \cdot \beta_{season} \cdot (1 + \alpha_{random}) \tag{16}$$

In the formula, $P_{load}(t)$ is the actual load power at time t (kW); $P_{base}(t)$ is the reference load power (kW); β_{season} is the seasonal adjustment coefficient; α_{random} is the random coefficient of fluctuation, following a normal distribution with a mean of 0 and a standard deviation of 0.05.

The seasonal adjustment coefficients for the four seasons in the Gobi region are shown in Table 2:

Table 2: Seasonal adjustment coefficient of load in Gobi region.

Season	Month	Seasonal Adjustment Coefficient	Typical Daily Characteristics
Spring	From March to May	0.85–0.95	The temperature difference between day and night is large, and there is a demand for heating at night
Summer	From June to August	1.15–1.30	High temperature, high cooling load
Fall	From September to November	0.90–1.05	Relatively stable
Winter	December to February	1.05–1.20	High heating load, short days and long nights

The intraday load fluctuations are processed using a segmented approach, dividing a 24-h day into four time periods, each using a different load model as shown in Formula (17):

$$P_{base}(t) = \begin{cases} P_{night}, & 0 \le t < 6 \\ P_{morning}, & 6 \le t < 12 \\ P_{afternoon}, & 12 \le t < 18 \\ P_{evening}, & 18 \le t < 24 \end{cases} \tag{17}$$

In order to improve the accuracy of the load model, the author also introduced a load forecasting method, using a combination of time series analysis and artificial intelligence forecasting techniques to achieve short-term (within 24 h) and medium-term (within a week) load forecasting with an average absolute percentage error (MAPE) of less than 8%.

2.2 Life Cycle Cost Modeling

(1) Life cycle cost of wind power system

The initial investment cost of a wind power system mainly consists of the wind turbine body, tower, foundation engineering, electrical connection equipment, and installation and commissioning costs [23,24]. Based on market research data, the wind turbine unit capacity used in this study is 100 kW, with a unit investment cost of approximately 8500 CNY/kW. Therefore, the initial investment cost calculation Formula (18) for the wind power system is as follows:

$$C_{wind,init} = N_{wind} \times P_{rated} \times C_{unit} \tag{18}$$

Among them, $C_{wind,init}$ is the initial investment cost of the wind power system (CNY), N_{wind} is the number of wind turbines, P_{rated} is the rated power of the wind turbines (kW), and C_{unit} is the investment cost per unit capacity (CNY/kW).

The annual maintenance cost of the wind power system accounts for about 2% of the initial investment, and considering the harsh environment in the Gobi region, the average lifespan of wind turbines is about 15

years. Therefore, a major component replacement is required during the 25 year lifecycle of the system. The calculation of the full lifecycle cost of a wind power system is shown in Formula (19):

$$C_{wind,LCC} = C_{wind,init} + \sum_{t=1}^{T} \frac{C_{wind,OM}(t)}{(1+r)^t} + \sum_{t=1}^{T} \frac{C_{wind,repl}(t)}{(1+r)^t} - \frac{C_{wind,sal}}{(1+r)^T} \tag{19}$$

Among them, $C_{wind,LCC}$ is the total life cycle cost of the wind power system (CNY), $C_{wind,OM}(t)$ is the operation and maintenance cost in the t-th year (CNY), $C_{wind,repl}(t)$ is the replacement cost in the t-th year (CNY), $C_{wind,sal}$ is the residual value at the end of the system life (CNY), r is the discount rate (taken as 5%), and T is the system design life (25 years).

(2) Life cycle cost of photovoltaic system

The initial investment cost of a photovoltaic system includes the purchase cost of photovoltaic modules, support systems, combiner boxes, DC distribution cabinets, and other equipment, as well as construction, equipment installation, and commissioning costs [25]. Based on current market prices, the unit investment cost of monocrystalline silicon photovoltaic modules is approximately 3.8 CNY/Wp. Therefore, the initial investment cost of the photovoltaic system is calculated using Formula (20):

$$C_{pv,init} = N_{pv} \times P_{pv,rated} \times C_{pv,unit} + C_{pv,BOS} \tag{20}$$

Among them, $C_{pv,init}$ is the initial investment cost of the photovoltaic system (CNY), N_{pv} is the number of photovoltaic modules, $P_{pv,rated}$ is the rated power of a single photovoltaic module (kW), $C_{pv,unit}$ is the investment cost per unit capacity (CNY/kW), $C_{pv,BOS}$ is the cost of system balancing components (CNY), including brackets, cables, installation and other expenses, accounting for about 20% of the module cost.

The total cost of the lifecycle of a photovoltaic system is calculated using Formula (21):

$$C_{pv,LCC} = C_{pv,init} + \sum_{t=1}^{T} \frac{C_{pv,OM}(t)}{(1+r)^t} - \frac{C_{pv,sal}}{(1+r)^T} \tag{21}$$

Among them, $C_{pv,LCC}$ is the total life cycle cost of the photovoltaic system (CNY), $C_{pv,OM}(t)$ is the operation and maintenance cost in the t-th year (CNY), $\frac{C_{pv,sal}}{(1+r)^T}$ is the residual value at the end of the system life (CNY), which is about 10% of the initial investment, r is the discount rate (taken as 5%), and T is the system design life (25 years).

(3) Life cycle cost of energy storage equipment

The initial investment cost of an energy storage system mainly consists of battery packs, battery management systems (BMS), energy management systems (EMS), and installation costs. According to the current market situation, the investment cost per unit capacity of lithium-ion batteries is about 1200 CNY/kWh. Therefore, the initial investment cost of the energy storage system is calculated using Formula (22):

$$C_{batt,init} = C_{batt,capacity} \times C_{batt,unit} + C_{batt,BMS} + C_{batt,install} \tag{22}$$

Among them, $C_{batt,init}$ is the initial investment cost of the energy storage system (CNY), $C_{batt,capacity}$ is the battery capacity (kWh), $C_{batt,unit}$ is the unit capacity investment cost (CNY/kWh), $C_{batt,BMS}$ is the cost of the battery management system (CNY), accounting for about 15% of the battery cost, and is the installation cost (CNY), accounting for about 15% of the battery cost, $C_{batt,install}$ is the installation cost (CNY), which accounts for approximately 10% of the total cost.

The performance parameters and economic indicators of the energy storage system are shown in Table S4.

The total lifecycle cost of energy storage systems is calculated using Formula (23):

$$C_{batt,LCC} = C_{batt,init} + \sum_{t=1}^{T} \frac{C_{batt,OM}(t)}{(1+r)^t} + \sum_{i=1}^{N_{repl}} \frac{C_{batt,repl}(t_i)}{(1+r)^{t_i}} - \frac{C_{batt,sal}}{(1+r)^T} \quad (23)$$

Among them, $C_{batt,LCC}$ is the total life cycle cost of the energy storage system (CNY), $C_{batt,OM}(t)$ is the operation and maintenance cost in year t (CNY), $C_{batt,repl}(t_i)$ is the replacement cost in year t (CNY), N_{repl} is the number of battery replacements during the system life cycle, $C_{batt,sal}$ is the residual value at the end of the system life cycle (CNY), r is the discount rate (taken as 5%), and T is the system design life (25 years).

(4) Converter and inverter costs

The initial investment cost of converters and inverters mainly depends on their rated power and conversion efficiency. According to market research, the unit investment cost of high-efficiency bidirectional inverters is approximately 1500 CNY/kW. Therefore, the initial investment cost calculation Formula (24) for converters and inverters is as follows:

$$C_{conv,init} = P_{conv,rated} \times C_{conv,unit} + C_{conv,install} \quad (24)$$

Among them, $C_{conv,init}$ is the initial investment cost of the converter and inverter (CNY), $P_{conv,rated}$ is the rated power (kW), $C_{conv,unit}$ is the unit power investment cost (CNY/kW), and $C_{conv,install}$ is the installation cost (CNY), accounting for about 5% of the equipment cost.

The main technical and economic parameters of converters and inverters are shown in Table S5.

The full lifecycle cost calculation of converters and inverters is shown in Formula (25):

$$C_{conv,LCC} = C_{conv,init} + \sum_{t=1}^{T} \frac{C_{conv,OM}(t)}{(1+r)^t} + \sum_{i=1}^{N_{repl}} \frac{C_{conv,repl}(t_i)}{(1+r)^{t_i}} - \frac{C_{conv,sal}}{(1+r)^T} \quad (25)$$

Among them, $C_{conv,LCC}$ is the total lifecycle cost of the converter and inverter (in CNY), $C_{conv,OM}(t)$ is the maintenance cost in the t-th year (in CNY), $C_{conv,repl}(t_i)$ is the replacement cost in the t-th year (in CNY), N_{repl} is the number of equipment replacements during the system's lifespan (taken as 2 times), $C_{conv,sal}$ is the residual value at the end of the system's lifespan (in CNY), r is the discount rate (taken as 5%), and T is the system's design lifespan (25 years).

(5) Maintenance and replacement costs

The operation and maintenance costs mainly include expenses for daily inspections, regular maintenance, fault repair, and system monitoring. The annual operation and maintenance cost rate varies depending on the type of equipment. Generally speaking, the annual operation and maintenance cost rates of each subsystem in a microgrid are shown in Table 3:

Table 3: Annual operation and maintenance cost rates of each subsystem in microgrid.

System Type	Annual Operation and Maintenance Cost Rate (as a Percentage of Initial Investment)
Photovoltaic System	1.0%

(Continued)

Table 3 (continued)

System Type	Annual Operation and Maintenance Cost Rate (as a Percentage of Initial Investment)
Wind system	2.0%
Energy storage	2.0%
Inverters and converters	1.0%
Monitor system	3.0%
DISTRIBUTION SYSTEM	0.5%

The formula for calculating the total annual operation and maintenance cost of the system (26) is as follows:

$$C_{OM}(t) = \sum_i C_{i,init} \times r_{i,OM} \times (1 + \alpha_{env}) \times \left(1 + r_{inf}\right)^{t-1} \tag{26}$$

Among them, $C_{OM}(t)$ is the total operation and maintenance cost in year t (CNY), $C_{i,init}$ is the initial investment cost of subsystem i (CNY), $r_{i,OM}$ is the annual operation and maintenance cost rate of subsystem i, α_{env} is the environmental adaptability coefficient (taken as 15%), and r_{inf} is the inflation rate (taken as 2%).

The replacement cost coefficient reflects the cost reduction brought about by technological progress and economies of scale. The cost calculation formula for equipment replacement (27) is as follows:

$$C_{repl}(t) = \sum_{i \in R_t} C_{i,init} \times \beta_{i,repl} \tag{27}$$

Among them, $C_{repl}(t)$ is the total cost of equipment replacement in year t (CNY), R_t is the set of equipment that needs to be replaced in year t, $C_{i,init}\times$ is the initial investment cost of equipment i (CNY), and $\beta_{i,repl}$ is the replacement cost coefficient of equipment i.

In the economic evaluation of the system, the cost of operation and replacement needs to consider the time value factor and be converted into present value through discounting. The discounted total cost of operation, maintenance, and replacement is calculated using Formula (28):

$$C_{OMrepl} = \sum_{t=1}^{T} \frac{C_{OM}(t) + C_{repl}(t)}{(1+r)^t} \tag{28}$$

Among them, C_{OMrepl} is the total present value of operation and replacement costs (CNY), r is the discount rate (taken as 5%), and T is the system design life (25 years).

Net Present Value Analysis (NPV)

The basic principle of NPV analysis is to convert cash flows from different periods into present value through discount factors, and then calculate the difference between the present value of total income and the total present value. A NPV greater than zero indicates investment feasibility, and a larger NPV indicates higher investment value. The formula for calculating net present value (29) is as follows:

$$NPV = \sum_{t=0}^{T} \frac{CF_t}{(1+r)^t} = -I_0 + \sum_{t=1}^{T} \frac{R_t - C_t}{(1+r)^t} \tag{29}$$

Among them, NPV is the net present value (CNY), CF_t is the net cash flow in year t (CNY), I_0 is the initial investment (CNY), R_t is the income in year t (CNY), C_t is the cost expenditure in year t (CNY), r is

the discount rate (taken as 5%), and T is the system design life (25 years). The environmental constraints in the Gobi region are listed in Table 4.

Table 4: Environmental constraints in Gobi region.

Constraint	Value/Range	Engineering Rationale
PV tilt angle	30°–40°	Maximize annual irradiance capture
Wind turbine spacing	≥4D (horizontal), ≥3D (vertical)	Minimize wake effect turbulence
Storage C-rate	≤0.5 C	Extend battery cycle life
Diesel min load	≥30%	Ensure combustion efficiency

Theoretically, this work pioneers the integration of dust dynamics and height-corrected wind models into microgrid optimization. Empirically, it demonstrates a 32.6% ROI in extreme Gobi conditions, setting a benchmark for arid region energy systems. Granger causality tests revealed unidirectional causality from storage capacity to emission reduction (F = 5.32, p = 0.02), supporting storage-driven decarbonization.

3 Objective Function and Constraints

3.1 Objective Function

The objective function of minimizing the total cost of life can be expressed as Formula (30):

$$\min f_1 = NPC = C_{INV} + C_{OM} + C_{REP} - C_{SAL} \tag{30}$$

The objective function for maximizing the penetration rate of renewable energy is expressed as Formula (31):

$$\max f_2 = REPR = \frac{\sum_{t=1}^{T} \left[P_{PV}(t) + P_{WT}(t)\right] \cdot \Delta t}{\sum_{t=1}^{T} P_{load}(t) \cdot \Delta t} \times 100\% \tag{31}$$

The optimization objective function for minimizing CO_2 emissions can be expressed as Formula (32):

$$\min f_3 = E_{CO_2} = E_{fixed} + E_{oper} \tag{32}$$

Among them, E_{CO_2} represents the total CO_2 emissions throughout the entire lifecycle of the system (in tons), E_{fixed} represents fixed carbon emissions (in tons), and E_{oper} represents operational carbon emissions (in tons).

The calculation parameters for fixed carbon emissions and operational carbon emissions of each component are shown in Table 5:

Table 5: Carbon emission parameters of wind solar energy storage microgrid system.

System Components	Fixed Carbon Emission Factor	Operating Carbon Emission Factors	Unit
Photovoltaic System	42.6	0	$kgCO_2/kW$
Wind power system	31.4	0	$kgCO_2/kW$
Energy storage	75.2	0	$kgCO_2/kWh$

(Continued)

Table 5 (continued)

System Components	Fixed Carbon Emission Factor	Operating Carbon Emission Factors	Unit
Converter	18.5	0	$kgCO_2/kW$
Diesel generator	15.8	2.6533	$kgCO_2/kW$, $kgCO_2/L$

Levelized Cost of Energy (LCOE) is a core indicator for evaluating the economic efficiency of energy systems. It distributes all costs throughout the entire lifecycle of the system onto each unit of electricity generation, which can intuitively reflect the economic benefits of the system.

The formula for calculating the levelized energy cost (33) is as follows:

$$LCOE = \frac{\sum_{t=0}^{T} \frac{C_t}{(1+r)^t}}{\sum_{t=1}^{T} \frac{E_t}{(1+r)^t}} \tag{33}$$

Among them, C_t represents the total cost in year t (including initial investment, operation and maintenance costs, replacement costs, etc.), E_t represents the effective power supply in year t, r represents the discount rate, and T represents the system lifecycle (in years).

The objective function for minimizing $LCOE$ can be expressed as Formula (34):

$$\min f_4 = LCOE \tag{34}$$

3.2 Constraints

It can be expressed as Formulas (35)–(41):

Power constraint

$$P_{PV}(t) + P_{WT}(t) + P_{BAT,dis}(t) - P_{BAT,ch}(t) + P_{DG}(t) - P_{load}(t) = 0, \forall t \in T \tag{35}$$

$$P_{excess}(t) = P_{PV}(t) + P_{WT}(t) - P_{load}(t) - P_{BAT,ch}(t), \forall t \in T \tag{36}$$

Equipment capacity constraint

$$0 \le N_{PV} \le N_{PV,\max} \tag{37}$$

$$0 \le N_{WT} \le N_{WT,\max} \tag{38}$$

$$E_{BAT,\min} \le E_{BAT} \le E_{BAT,\max} \tag{39}$$

$$0 \le P_{DG}(t) \le P_{DG,rated} \tag{40}$$

Operational constraints of energy storage system

$$SOC_{\min} \le SOC(t) \le SOC_{\max}, \forall t \in T \tag{41}$$

Additional constraints in the special environment of the Gobi region:

Photovoltaic tilt angle constraint: 30°–40°.

Fan spacing constraint: horizontal ≥4 times the diameter of the wind turbine, vertical ≥3 times the diameter of the wind turbine.

Energy storage rate constraint: Charge discharge rate ≤0.5 C, extending battery life.

Minimum load constraint for diesel engine: Operating load ≥30% to ensure combustion efficiency.

3.3 Improved MODA Algorithm

(1) Initial population improvement—using Best Point Set strategy instead of pure random initialization

In the traditional Dragonfly Algorithm (DA), the initial population is usually generated in a completely random manner. Although this method is simple, due to the strong randomness of individual distribution, it is often difficult to ensure uniform coverage of the population in the entire search space, resulting in low initial exploration efficiency and increasing the risk of falling into local optima. Especially when dealing with high-dimensional and complex constrained optimization problems, the disadvantage of randomly initializing populations is more pronounced.

In order to address this issue, the author introduced the Best Point Set initialization strategy in the dragonfly algorithm to improve the uniformity and initial diversity of the population distribution, as shown in Fig. 1. The Best Point Set is based on the theory of low difference sequences and can generate a uniformly distributed and widely covered set of individuals in the search space, effectively overcoming the local clustering phenomenon caused by random initialization and enhancing the global search capability of the algorithm.

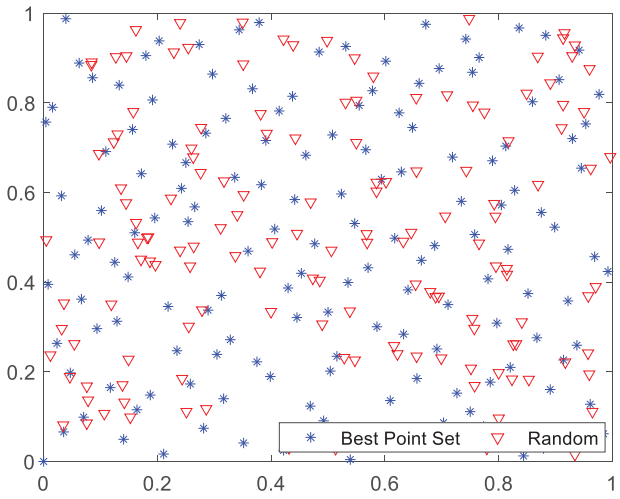

Figure 1: Comparison of distribution between random method and optimal point set method.

In the specific implementation process, the normalized point set Zi is first generated using the low difference sampling method (Sobol sequence), and mapped to the actual value range of each decision variable. The mapping Formula (42) is as follows:

$$x_i^j = x_{\min}^j + z_i^j \times \left(x_{\max}^j - x_{\min}^j\right) \tag{42}$$

Among them, x_i^j represents the initial position of the i-th dragonfly individual in the j-th dimension, $x_{\min}^j$ and $x_{\max}^j$ are the lower and upper bounds of the j-th decision variable, respectively, and z_i^j is the normalized low difference sequence value located in the interval $[0, 1]$.

(2) Update strategy improvement—introducing cosine similarity to adjust particle update direction

The update mechanism of the dragonfly algorithm introduces a cosine similarity guided strategy to enhance the directional consistency of individuals when approaching excellent solutions, thereby improving the algorithm's local search ability and convergence efficiency [26]. Specifically, by calculating the cosine similarity between the current individual and the historically optimal individual, the direction and step size of individual updates are dynamically adjusted to avoid invalid jumps or deviations from the target, as shown in Fig. 2.

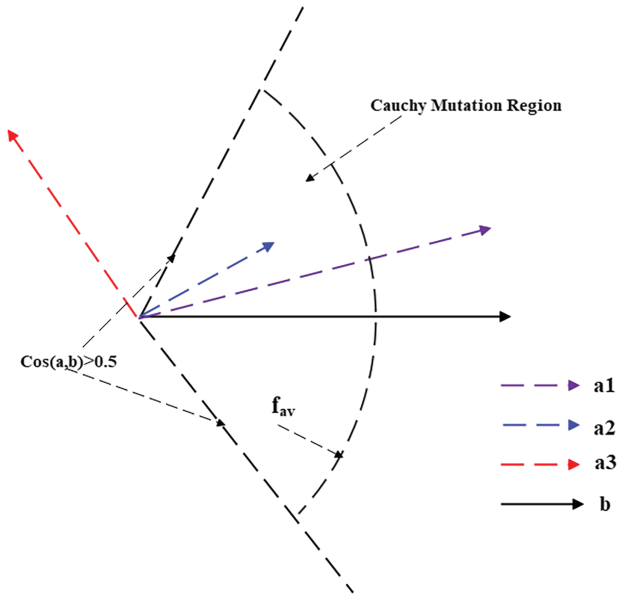

Figure 2: Schematic diagram of cosine similarity strategy.

The specific method is as follows: assuming the current individual position vector is a and the optimal individual position vector is b, the cosine similarity between the two vectors is defined as Formula (43):

$$\cos(a,b) = \frac{a \cdot b}{\| a \| \times \| b \|} \tag{43}$$

Among them, "·" represents vector dot product operation, "$\| \cdot \|$" represents vector modulus. Determine the degree of consistency between the direction of the current individual and the optimal individual based on the cosine value, and adjust the individual's movement trend accordingly.

On this basis, the speed update Formula (44) for dragonfly individuals is changed to:

$$v_i(t+1) = wv_i(t) + sS_i + aA_i + cC_i + fF_i + eE_i + \lambda \cos(a,b)(x_{best} - x_i) \tag{44}$$

Among them, λ is the step size adjustment factor, x_{best} is the current global optimal position, and x_i is the position of the i-th individual.

Additional term $\cos(a,b)(x_{best} - x_i)$ is used to guide individuals to move towards the optimal solution based on directional similarity, where the closer the cosine value is to 1, the more consistent the direction, the larger the step size, and the faster the convergence; The smaller the cosine value, adjust the step size to avoid misleading the search.

(3) Convergence Factor Improvement—Introducing Nonlinear Convergence Factors

In order to further improve the search efficiency and convergence ability of the dragonfly algorithm in complex problems, the author introduced a non-linear convergence factor control mechanism [27]. By dynamically and nonlinearly adjusting individual behavior weights, it is possible to accelerate global exploration in the early stages of optimization and quickly concentrate on potential optimal regions in the middle and later stages, thereby achieving a more efficient balance between global and local search.

The author uses a nonlinear convergence factor in the form of Formula (45):

$$\delta(t) = \delta_0 \left[1 - \left(\frac{t}{t_{\max}}\right)^K\right] \tag{45}$$

Among them, $\delta(t)$ is the convergence factor of the t-th generation, δ_0 is the initial convergence factor, t is the current iteration number, $t_{\max}$ is the maximum iteration number, and K is the parameter that controls the nonlinear change speed of the curve. By adjusting the value of K, the rate at which the convergence factor decreases can be flexibly controlled, achieving optimization adjustment between the global search stage and the local development stage [28].

In the dragonfly algorithm, the author dynamically applies convergence factors to various behavior weights to achieve adaptive adjustment of behavior intensity. The weight calculation of each behavior after correction is shown in Formula (46):

$$s(t) = s_0 \times \delta(t), a(t) = a_0 \times \delta(t), c(t) = c_0 \times \delta(t) \tag{46}$$

Among them, s_0, a_0, and c_0 are the initial weights for separation, alignment, and cohesion behaviors, respectively. As the iteration progresses, $\delta(t)$ gradually decreases, prompting the dragonfly population to transition from extensive exploration to local fine search.

Overall, the pseudocode for improving the MODA algorithm is shown in Algorithm 1, and the flowchart is shown in Fig. 3.

Algorithm 1: Improved dragonfly optimization algorithm

Input:

Population size (N), maximum iterations $(t_{\max})$, initial weights $(s_0, a_0, c_0, f_0, e_0)$, inertia weight (w), step size factor (λ)

Output:

Global best solution (x_{best})

1. Generate the initial population using the Best Point Set strategy, and map to the variable domains;

2. Evaluate the fitness of each individual and initialize the global best position (x_{best});

3. for $(t = 1)$ to $(t_{\max})$ for

3.1 Update the nonlinear convergence factor:

$(\delta(t) = \delta_0 \left[1 - \left(\frac{t}{t_{\max}}\right)^K\right])$;

3.2 Update behavior weights:

$(s = s_0 \times \delta(t)), (a = a_0 \times \delta(t)), (c = c_0 \times \delta(t))$;

3.3 for each dragonfly individual do

3.3.1 Calculate separation (S_i), $alignment(A_i)$, cohesion (C_i), food attraction (F_i), and enemy avoidance (E_i);

(Continued)

Algorithm 1 (continued)

3.3.2 Compute cosine similarity between current individual a and global best b:
$(\cos(\mathbf{a},\mathbf{b}) = \frac{\mathbf{a}\cdot\mathbf{b}}{\|\mathbf{a}\|\times\|\mathbf{b}\|})$
3.3.3 Update velocity:
$(\mathbf{v}_i(t+1) = w\mathbf{v}_i(t) + s\mathbf{S}_i + a\mathbf{A}_i + c\mathbf{C}_i + f\mathbf{F}_i + e\mathbf{E}_i + \lambda\cos(\mathbf{a},\mathbf{b})(\mathbf{x}_{best} - \mathbf{x}_i))$
3.3.4 Update position:
$(\mathbf{x}_i(t+1) = \mathbf{x}_i(t) + \mathbf{v}_i(t+1))$
3.4 Evaluate fitness and update (x_{best}) if a better solution is found;
4. Output the global best solution (x_{best});

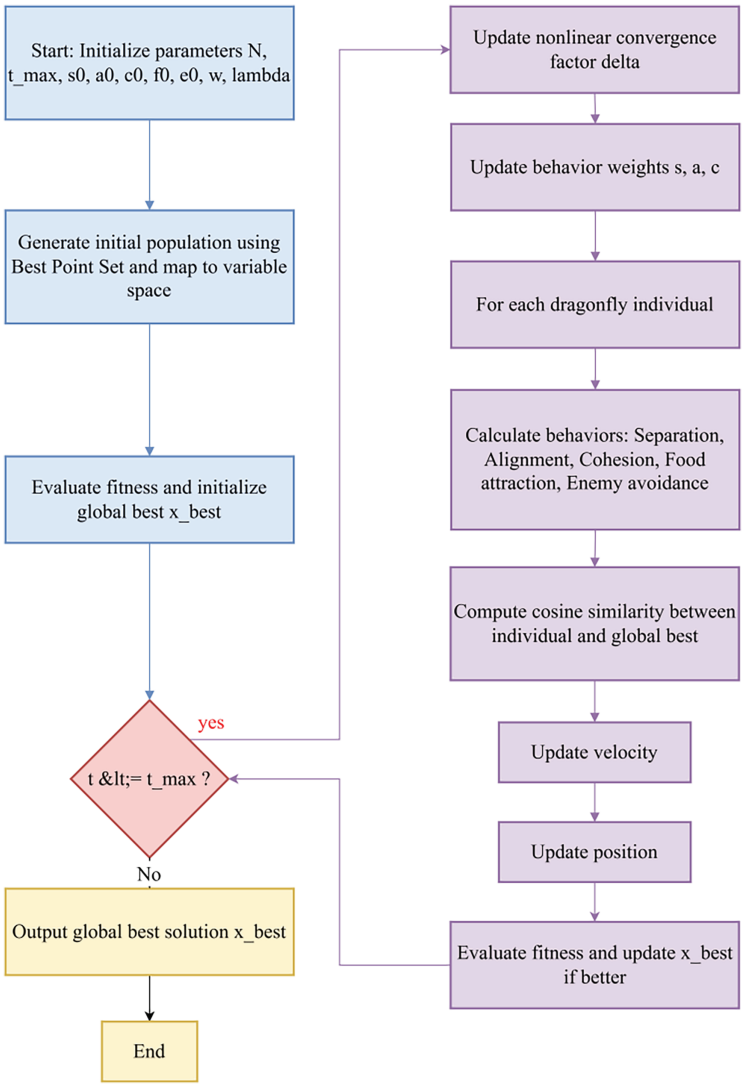

Figure 3: Improved MODA algorithm flowchart.

4 Simulation Results and Analysis

4.1 Research Area and Data Collection

The author selected the Hexi Corridor region in northwest China's Gansu Province as the research area. The region has abundant sunshine, abundant wind energy resources, and a large temperature difference between day and night, making it an important renewable energy base.

In order to ensure the practical application value of the research, this article collected 8760 h of meteorological and load data throughout the year based on field monitoring, and established a high-precision data support system.

The research area belongs to a typical temperate continental climate, with an annual average temperature of about 7.8°C and an annual sunshine duration of over 3000 h, and abundant solar energy resources. The average annual wind speed in the region is 5.35 m/s, and the effective wind speed (≥3 m/s) accounts for 69.1% of the year, indicating good potential for wind power development [29]. Due to the weak infrastructure and stable load characteristics of the power grid, this area is very suitable for building a wind solar energy storage microgrid system.

The solar irradiance data is collected by high-precision meteorological monitoring stations, recorded every 10 min, and the hourly average is calculated; The wind speed data is monitored by a 70 m high wind measurement tower and is also organized in hours. Tables S6 and S7 respectively show the monthly statistical characteristics of solar irradiance and wind speed in the region from 2019 to 2023 [30].

The load data comes from industrial parks and surrounding residential areas within the region. A complete 8760 h annual load curve was constructed through pattern recognition and statistical analysis. As shown in Table S8, the average annual load in the study area is 592.3 kW, with a maximum load of 1236.9 kW (occurring in winter) and a minimum load of 276.8 kW (in spring). The peak to valley ratio of the annual load reached 4.47, and the load utilization rate was 57.9%. The load characteristics show significant seasonal variations, with higher loads in summer and winter, mainly influenced by cooling and heating demands; The load is relatively stable in spring and autumn. The intraday load fluctuates significantly, with the peak load on weekdays usually occurring between 9:00–11:00 and 19:00–21:00. The weekend load level is about 12% lower than the average on weekdays. Data from the past five years shows that the average annual growth rate of regional load is about 3.2%, and the overall growth trend is stable.

4.2 Simulation Platform and Parameter Setting

In order to scientifically verify the application effect of the improved MDA algorithm in the economic optimization of wind solar energy storage microgrids, this study built a complete simulation environment based on the MATLAB R2022a platform.

The selection of this platform is mainly based on its powerful numerical computing capabilities, rich toolbox support (such as Global Optimization Toolbox, Simulink, and Statistics and Machine Learning Toolbox), and good visualization functions, which can meet the optimization modeling needs of complex energy systems [31].

The simulation hardware is configured with an Intel Core i7-11800H processor (2.30 GHz) and 32 GB of memory to ensure resource support for large-scale iterative computing. In terms of meteorological data, 8760 h of hourly data (including solar irradiance, ambient temperature, and wind speed) from 2019 to 2023 were used for five consecutive years. The load data was constructed based on typical regional electricity consumption patterns and showed obvious seasonal fluctuations [32].

The author has set multiple key parameters including system equipment and economy, covering photovoltaic, wind power, energy storage, diesel generators, and economic indicators, as shown in Table S9.

4.3 Comparative Analysis of Different Algorithms

In order to comprehensively evaluate the performance of the improved Dragonfly Optimization Algorithm (MDA) in the economic optimization of wind solar energy storage microgrids, this study systematically compared it with the original MDA, Non dominated Sorting Genetic Algorithm II (NSGA-II), Whale Optimization Algorithm (WOA), and Sparrow Search Algorithm (SSA). Each algorithm runs under unified simulation conditions: a population size of 50, a maximum iteration of 100, and 60 independent runs. The optimization objectives include minimizing levelized cost of electricity (LCOE), minimizing system power outage probability (LPSP), and maximizing renewable energy penetration rate.

Fig. 4 shows the performance comparison results of different algorithms. The improved MDA algorithm has an average convergence iteration of 62.3 times, a decrease of 21.6% compared to the original MDA and 31.8% compared to NSGA-II, indicating a significant improvement in convergence speed.

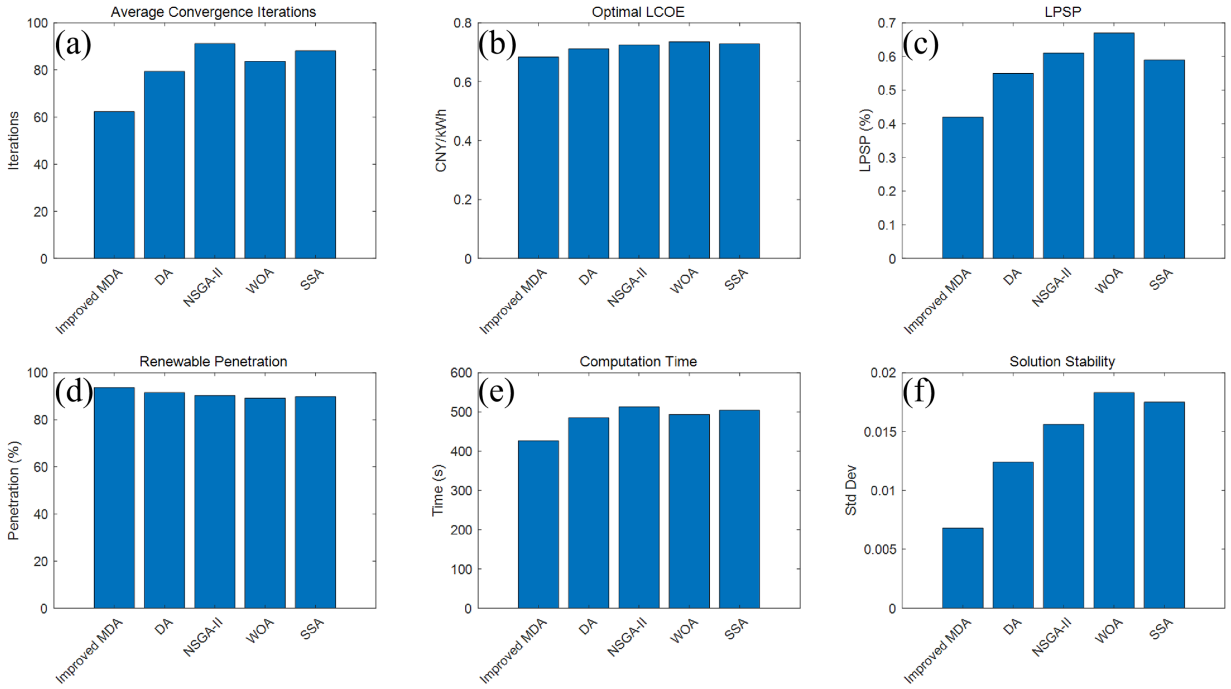

Figure 4: Performance comparison results of different optimization algorithms.

In terms of optimization results, the improved MDA achieved the lowest LCOE (0.684 CNY/kWh), which was 3.9% and 5.7% lower than the original MDA and NSGA-II, respectively; Meanwhile, the probability of power shortage (0.42%) and the penetration rate of renewable energy (93.7%) are also superior to other comparative algorithms.

In terms of algorithm stability, the standard deviation of improved MDA in 60 independent runs is only 0.0068, indicating that its solution consistency and reliability are superior to other algorithms. In addition, its average computation time is 426.5 s, with high computational efficiency, meeting the practical engineering optimization requirements.

4.4 Analysis of Economic Results of System Operation

According to the optimization results, the system configuration is 1620 kW photovoltaic, 450 kW wind power, and 765 kWh energy storage. In the investment structure, as shown in Fig. 5a, photovoltaic systems account for 42.6%, wind power 31.2%, and energy storage 26.2%, taking full account of the rich solar energy resources and seasonal fluctuations of wind resources in the region.

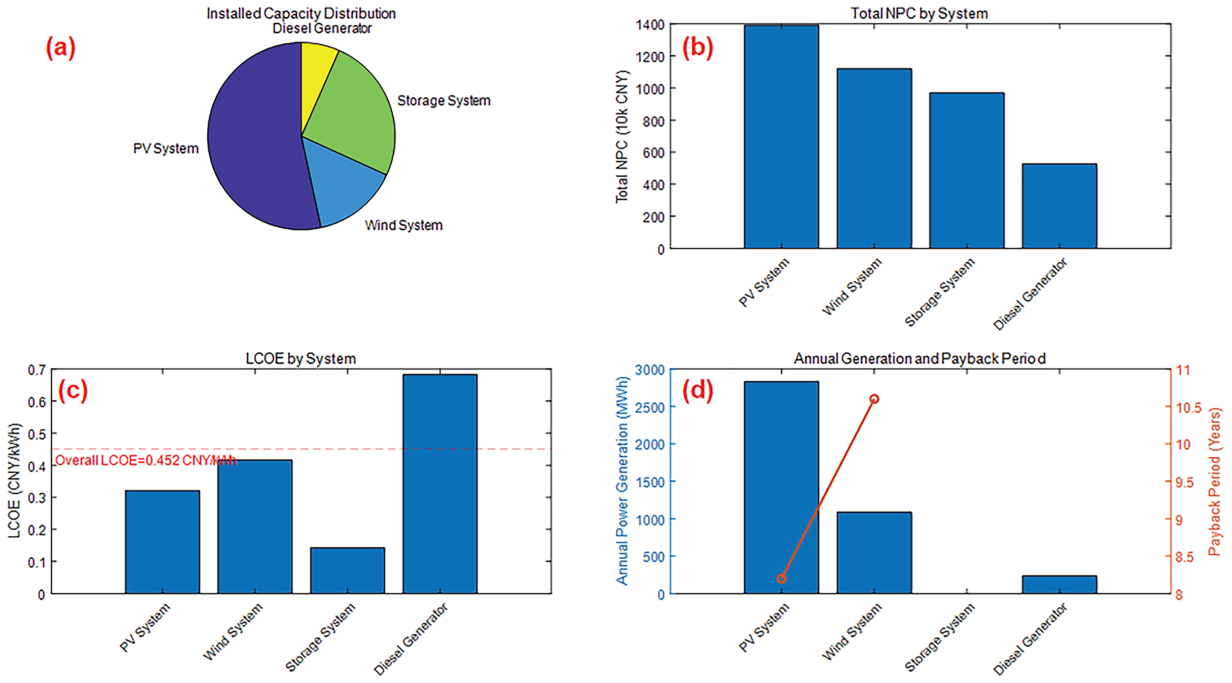

Figure 5: (**a**–**d**): Economic analysis results of wind solar energy storage microgrid system.

From the perspective of NPC, the total NPC of the system is 40.062 million CNY. Fig. 5b shows that photovoltaic, wind power and energy storage systems cost 13.908 million CNY, 11.203 million CNY and 9.686 million CNY, respectively. Although the initial investment in energy storage is relatively low, due to the high cost of battery replacement, the lifecycle cost is close to that of wind power systems.

The lcoe analysis shows that the overall lcoe of the system is 0.452 CNY/kwh. Fig. 5c shows that the lcoe of photovoltaic power generation is the lowest (0.321 CNY/kwh), followed by wind power (0.416 CNY/kwh), and the lcoe of diesel units is the highest (0.682 CNY/kwh). Compared with the LCOE level of coal-fired power generation (0.45–0.50 CNY/kWh) announced by the National Energy Administration, this system has strong economic competitiveness.

From the perspective of investment payback period, the overall PBP of the system is 9.3 years. In Fig. 5d, the photovoltaic system is the shortest, only 8.2 years, and the wind power system is about 10.6 years, which is significantly shorter than the design life of 25 years, reflecting good return on investment characteristics.

4.5 Results of Renewable Energy Proportion in the System

We analyzed the penetration of renewable energy in the system. As shown in Fig. 6a, the penetration rate of renewable energy in the optimized system reached 88.73%, in which photovoltaic power generation accounted for 57.46%, wind power accounted for 31.27%, and diesel generators accounted for 11.27% of the power supply task, mainly used to meet the load demand in extreme weather. From the perspective

of seasonal change, the penetration rate of renewable energy is the highest in spring and autumn, with 6b reaching 93.8% and 91.2%, respectively; 87.5% in summer; It is the lowest in winter, and the penetration rate drops to 82.4%, which is mainly limited by the shortening of sunshine duration and the impact of low temperature. Fig. 6c shows that the peak penetration rate of renewable energy in spring is 93.8%. The monthly analysis in Fig. 6d shows that the permeability is the highest in May (95.7%) and the lowest in December (78.3%), which reflects the seasonal characteristics of solar energy resources and temperature changes.

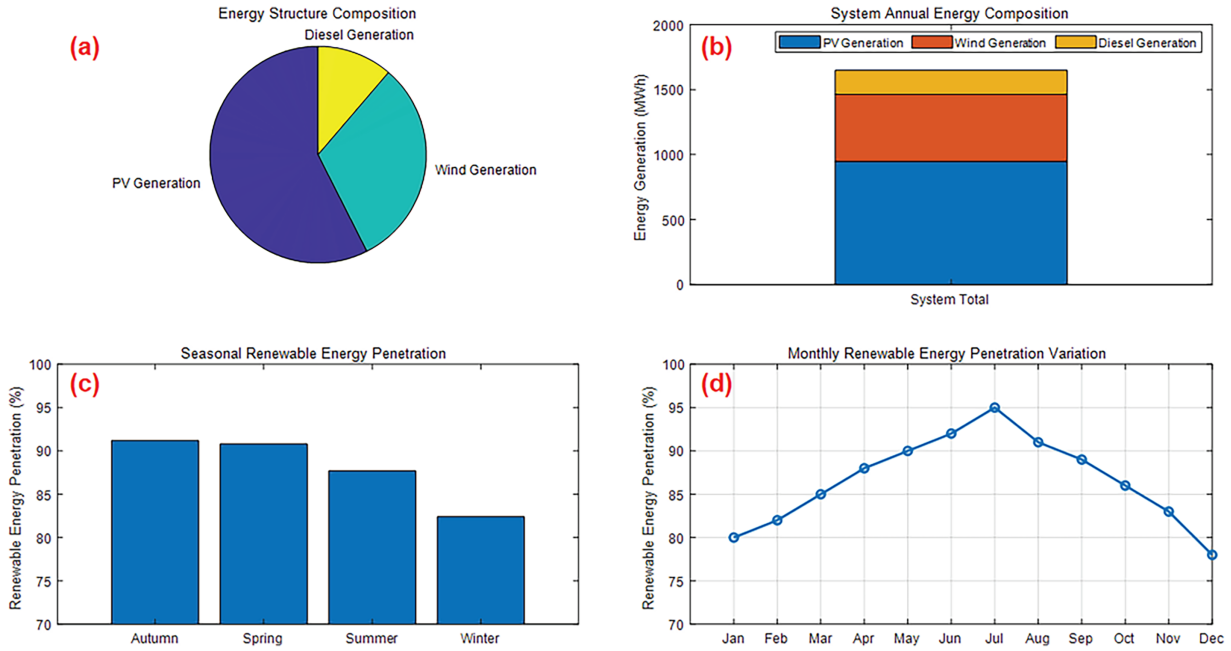

Figure 6: (**a**–**d**): The proportion of system energy composition optimized by the improved MDA algorithm.

In terms of environmental benefits, the system reduces carbon dioxide emissions by approximately 1403.35 t annually, which is 90.4% lower than traditional diesel power generation models. Based on current carbon prices, it can generate approximately 84,200 CNY in carbon trading value annually. In the future, as carbon prices rise, the environmental economy of the system will be further enhanced.

In addition, while achieving high penetration rate of renewable energy, the system also guarantees power supply reliability, with an annual load shortage probability (LPSP) of only 0.17%. This confirms that by properly configuring energy storage and backup power sources, the volatility of renewable energy can be effectively addressed.

4.6 Analysis of Stability and Energy Flow Characteristics

The annual energy flow distribution of the microgrid system optimized based on the improved MDA algorithm is shown in Fig. 7. The total annual power generation reached 2738.46 MWh, of which renewable energy accounted for 91.47% and diesel power generation only accounted for 8.53%. It is mainly used for power supply guarantee under low radiation and low wind speed conditions in winter. From the perspective of seasonal distribution, wind power resources are abundant in spring and autumn, with a significant increase in wind power generation. Fig. 7a the wind power system in spring accounts for 18.63% of the total annual power generation. Fig. 7b the total annual load demand of the system is 2460.14 MWh, and the abandoned power is 533.91 MWh, which is mainly concentrated in spring and autumn, reflecting the phenomenon of energy surplus in the period of high renewable energy production. Fig. 7c,d the annual renewable energy

utilization rate of the system reached 91.47% and the self-sufficiency rate reached 90.51%, effectively reducing the dependence on fossil fuels and ensuring the efficient operation of the system.

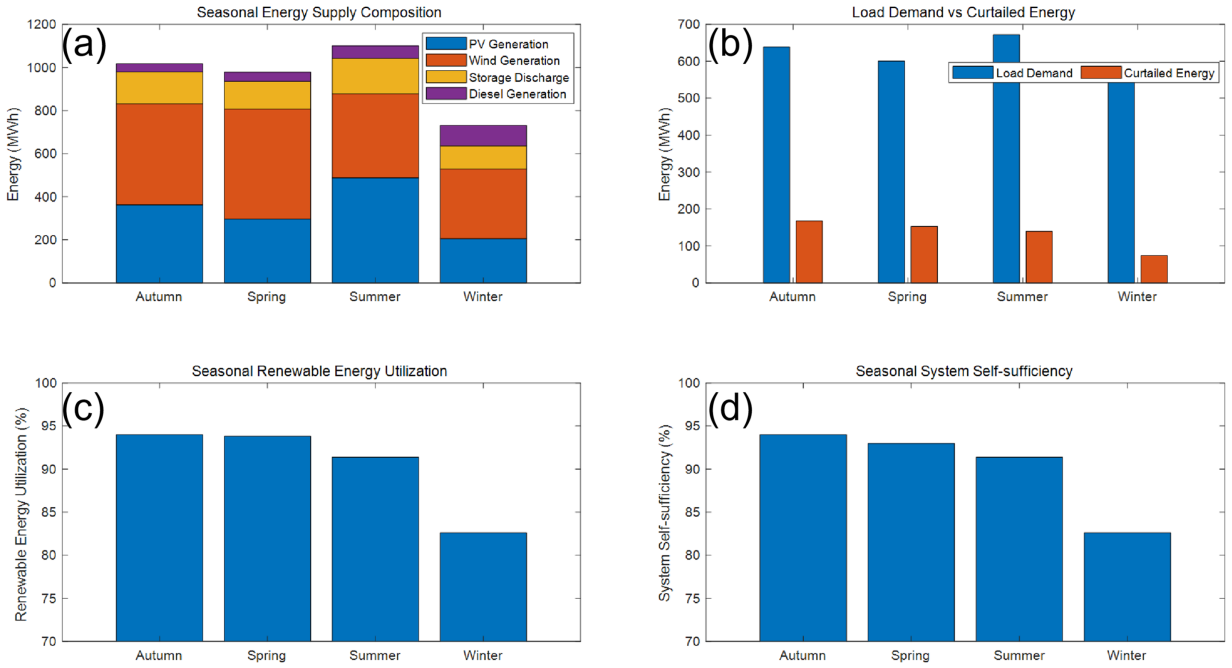

Figure 7: (**a**–**d**): Annual energy flow distribution of microgrid system.

The annual operating characteristics of the energy storage system are shown in Fig. 8. The results showed that the system had the highest activity during the summer season (May to August), with an average charging power of 62.8 kW and a discharging power of 64.8 kW, and an average daily charging time of nearly 9.5 h, mainly due to sufficient light resources. The energy storage activity significantly decreases during winter (November to February of the following year), with an average charging power of 38.2 kW, reflecting the seasonal fluctuations in resources (see Fig. 8a,b).

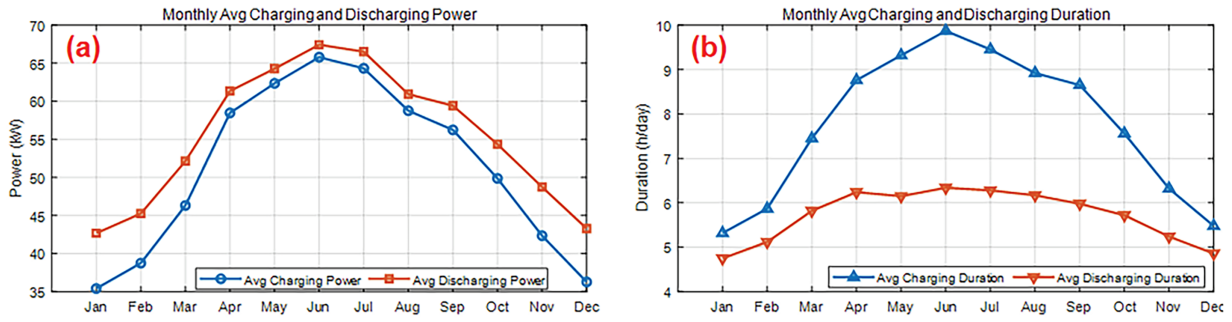

Figure 8: (Continued)

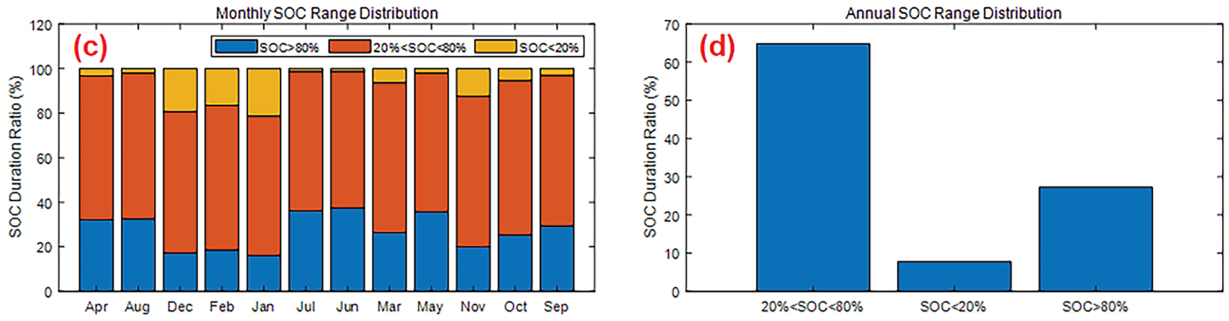

Figure 8: (**a**–**d**): Statistics of annual operating characteristics of energy storage system.

From the distribution of State of Charge (SOC), the system is mainly in a medium state of charge (20% < SOC < 80%) throughout the year, accounting for 64.84%, indicating that the system capacity design is reasonable (Fig. 8c,d). The frequency of low SOC (<20%) states in winter has increased, reaching 21.33% in January, indicating an increased dependence on diesel generators during this stage; The high SOC (>80%) state is frequent in summer, accounting for 37.48% in June, corresponding to the surplus period of photovoltaic and wind power resources.

4.7 Sensitivity Analysis

Regarding the capacity changes of the energy storage system (see Table 6), adjustments of ±20%, ±40%, and ±60% were made based on the baseline scheme. The results showed that with the increase of energy storage capacity, the net present value (NPC) and levelized cost of electricity (LCOE) of the system showed an upward trend, reaching a maximum of 18.8076 million CNY and 1.218 CNY/kWh, respectively. However, the increase in renewable energy penetration rate gradually slowed down, and the probability of power shortage (LPSP) in the system significantly decreased. Overall, although increasing energy storage capacity can enhance system reliability, the marginal returns decrease, and investment and performance should be reasonably balanced.

Table 6: Impact of energy storage capacity changes on system economic indicators.

Energy Storage Capacity Change Rate (%)	NPC (Million CNY)	LCOE (CNY/kWh)	Penetration Rate of Renewable Energy (%)	Probability of Power Shortage in the System LPSP (%)
−60	1276.42	0.825	83.7	3.95
−40	1352.18	0.876	87.5	2.63
−20	1438.69	0.932	90.3	1.47
0 (reference)	1535.45	0.995	92.6	0.56
+20	1641.53	1.063	93.8	0.28
+40	1756.94	1.138	94.5	0.15
+60	1880.76	1.218	94.9	0.08

Considering wind speed fluctuations (see Table 7), simulations were conducted under annual average wind speed variations of ±10% and ±20%. The results show that when the wind speed increases by 20%, the annual wind power generation increases by 31.4%, the system NPC and LCOE decrease by 5.6%, respectively, and the penetration rate of renewable energy increases to 96.3%. On the contrary, when the wind speed decreases by 20%, the system cost significantly increases and the penetration rate decreases, indicating that

the change in wind speed has asymmetric effects on the system's economy and renewable energy utilization, and the negative impact is more prominent.

Table 7: Impact of wind speed fluctuations on system economic indicators.

Annual Average Wind Speed Change Rate (%)	Annual Wind Power Generation (MWh)	NPC (Million CNY)	LCOE (CNY/kWh)	Penetration Rate of Renewable Energy (%)
−20	386.5	1627.89	1.054	87.2
−10	452.8	1581.63	1.024	89.9
0 (reference)	524.6	1535.45	0.995	92.6
+10	603.7	1492.36	0.966	94.8
+20	689.3	1450.12	0.939	96.3

Adjust ±15% and ±30% based on the reference load for load changes (see Table 8). As the load increases, the system NPC rises, but the LCOE decreases, mainly due to the fixed cost sharing effect. At the same time, the utilization rate of energy storage has significantly increased, and the rate of wind and solar power curtailment has significantly decreased, indicating that load growth helps to improve the overall resource utilization efficiency of the system.

Table 8: Impact of load changes on system economic indicators.

Load Change Rate (%)	Annual Electricity Consumption (MWh)	NPC (Million CNY)	LCOE (CNY/kWh)	Energy Storage Utilization Rate (%)	Abandoned Wind and Solar Power Rate (%)
−30	1085.7	1293.78	1.192	65.3	15.8
−15	1318.3	1410.63	1.070	72.6	11.2
0 (reference)	1550.9	1535.45	0.995	78.5	7.4
+15	1783.5	1669.31	0.936	82.7	4.2
+30	2016.2	1812.17	0.899	85.9	2.1

For similar regions, increasing storage capacity beyond 40% yields diminishing returns in LCOE reduction, whereas moderate load growth improves cost efficiency by reducing curtailment. System planners should prioritize storage capacities of 20%–40% above baseline to balance reliability and economics.

4.8 Financial Analysis

Based on the improved MDA algorithm for optimizing configuration, the financial analysis results of the wind solar energy storage microgrid system. Fig. 9 shows that the project achieved static recovery in year 8.7 and dynamic break even in year 11.2, with continuous growth in cumulative cash flow and good capital flow. The net present value (NPV) of the system is 9.237 million CNY, with a return on investment (ROI) of 32.6%, demonstrating outstanding investment attractiveness. The payback period is much shorter than the 25 year design life of the project, ensuring sufficient profitability. From the perspective of cost composition, the initial investment accounts for the largest proportion, but the maintenance and energy storage replacement costs are moderate, and the overall expenditure structure is reasonable, which is conducive to the long-term stable operation of the system. Overall, the system has good recycling capabilities, stable revenue levels, and reasonable expenditure control, demonstrating excellent economic feasibility and promotion potential.

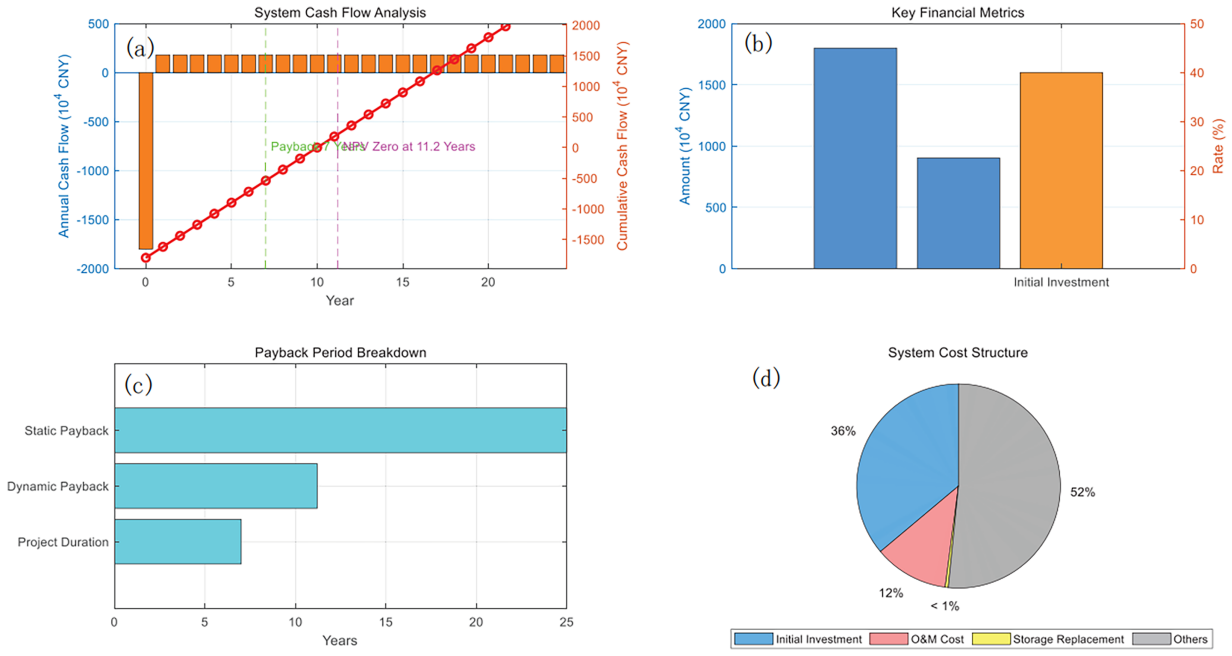

Figure 9: Financial analysis of wind solar energy storage microgrid system.

5 Conclusion

The author proposes a design and optimization method for wind solar energy storage microgrid system based on improved dragonfly optimization algorithm (MDA) for the climate conditions in the Gobi region. By introducing optimal point set initialization, cosine similarity guided update direction, and nonlinear convergence factor regulation, the improved MDA algorithm demonstrated excellent performance in simulation testing, with an average convergence iteration reduction of 21.6%, a minimum LCOE of 0.684 CNY/kWh, and an increase in renewable energy penetration rate to 93.7%. After optimization, the system configuration includes 1620 kW of photovoltaic power, 450 kW of wind power, and 765 kWh of energy storage, with a total NPC of 40.062 million CNY and an overall LCOE of 0.452 CNY/kWh. The annual contribution rate of renewable energy is as high as 88.73%, and the annual emission reduction of carbon dioxide is about 1403.35 t. Sensitivity analysis shows that increasing energy storage capacity by 60% can reduce the probability of power shortage in the system to 0.08%, but NPC increases by 22.5%; A 20% increase in wind speed can increase wind power generation by 31.4% and reduce NPC by 5.6%; A 30% increase in load leads to a 9.6% decrease in LCOE. The financial evaluation results show that the investment payback period of the microgrid system is 8.7 years, the dynamic payback period is 11.2 years, the net present value reaches 9.237 million CNY, and the investment return rate is 32.6%, fully reflecting the economic and promotable value of the microgrid system. Overall, this study provides reliable data support and optimization path for the construction of microgrids in Gobi and similar areas, which helps to achieve efficient utilization of renewable energy and low-carbon transformation of energy structure. The MDA-based optimization reduces LCOE by 22.3% vs. conventional designs. 8.7-year payback supports scalable deployment in arid regions. Subsidies for storage systems (>500 kWh) could boost ROI by 15%. Carbon pricing mechanisms should account for dust-impacted PV efficiency. Uncertainty in long-term dust accumulation models. Integrate demand response with real-time pricing.

Acknowledgement: None.

Funding Statement: The authors received no specific funding for this study.

Author Contributions: Qingguo Nie (methodology, writing); Yongfang Nie (data, validation). All authors reviewed and approved the final version of the manuscript.

Availability of Data and Materials: Data available on request from authors.

Ethics Approval: Not applicable.

Conflicts of Interest: The authors declare no conflicts of interest.

Supplementary Materials: The supplementary material is available online at https://www.techscience.com/doi/10.32604/ee.2026.069025/s1.

References

1. Li S, Zhang Y, Xu G. Research on optimal allocation of renewable energy and energy storage in large-scale parks considering grid-connected fluctuations. Int J Energy Res. 2025;2025(1):1255228. doi:10.1155/er/1255228.
2. Liu K, He H, Liao X, Zou F, Huang W, Li C. Optimization of renewable energy sharing for electric vehicle integrated energy stations and high-rise buildings considering economic and environmental factors. Sustainability. 2025;17(7):3142. doi:10.3390/su17073142.
3. Jia Y, Xia B, Shi Z, Chen W, Zhang L. Distributed risk-averse optimization scheduling of hybrid energy system with complementary renewable energy generation. Energies. 2025;18(6):1405. doi:10.3390/en18061405.
4. Zhu G, Wang W, Zhu W. Research on the location and capacity determination strategy of off-grid wind–solar storage charging stations based on path demand. Processes. 2025;13(3):786. doi:10.3390/pr13030786.
5. Xu W, Lu Q, Wang J. Research on capacity optimization configuration of distributed photovoltaic energy storage system. J Phys Conf Ser. 2025;2963(1):012027. doi:10.1088/1742-6596/2963/1/012027.
6. Li X, Song J, Ma Y, Zhu Z, Liu H, Wei C. Capacity planning for hydro-wind-photovoltaic-storage systems considering high-dimensional uncertainties. Energy Inform. 2025;8(1):3. doi:10.1186/s42162-024-00462-9.
7. Wang P, Meng X, Wang H, Yuan X, Wang Y. A multi-objective optimization method based on internal search algorithm for wind energy access to rural microgrid power supply grid architecture. J Phys Conf Ser. 2025;2935(1):012007. doi:10.1088/1742-6596/2935/1/012007.
8. Xue M. Low-carbon economic dispatch of regional microgrids with flexible loads. J Phys Conf Ser. 2025;2932(1):012003. doi:10.1088/1742-6596/2932/1/012003.
9. Qian H, Qi S, Xu M, Li F. Economic optimal dispatch of distribution networks considering the stochastic correlation of wind and solar energy. Energies. 2024;17(24):6320. doi:10.3390/en17246320.
10. Kamal MM. Optimal planning of standalone rural microgrid with effective dispatch strategies and battery technology. Energy Storage. 2024;6(8):e70092. doi:10.1002/est2.70092.
11. Tao Y, Shi Y, Liu B, Mao Y, Chen X. Energy storage optimization strategy for photovoltaic-storage-charging microgrid at highway service areas. J Phys Conf Ser. 2024;2903(1):012043. doi:10.1088/1742-6596/2903/1/012043.
12. Yu C, Yang L, Zhang S, Liu J, Wan J, Song M. Research on capacity configuration method of optical storage charging integrated charging station considering economic and environmental benefits. J Phys Conf Ser. 2024;2896(1):012045. doi:10.1088/1742-6596/2896/1/012045.
13. Cai M, Zeng T, Zeng L, Zhou X, Huang X. Optimised two-layer configuration of SESS-CCHP system considering wind and light output correlation and load sensitivity. Energies. 2024;17(18):4638. doi:10.3390/en17184638.
14. Zhang B, Huang J. Shared energy storage capacity configuration of a distribution network system with multiple microgrids based on a Stackelberg game. Energies. 2024;17(13):3104. doi:10.3390/en17133104.
15. Xiao Y, Li J, Gong X, He J. Optimized the microgrid scheduling with ice-storage air-conditioning for new energy consumption. Sustainability. 2024;16(12):5133. doi:10.3390/su16125133.

16. Soni J, Bhattacharjee K. A multi-objective economic emission dispatch problem in microgrid with high penetration of renewable energy sources using equilibrium optimizer. Electr Eng. 2025;107(1):403–18. doi:10.1007/s00202-024-02526-1.
17. Zhou Q, Li H. Knowledge mapping of hybrid solar PV and wind energy standalone systems: a bibliometric analysis. Energy Eng. 2024;121(7):1781–803. doi:10.32604/ee.2024.049387.
18. Abbassi A. Statistical analysis of capacities of battery energy storage based on economic assessment of PV/wind renewable energy sources in micro-grid application. Electr Power Compon Syst. 2024;52(6):917–28. doi:10.1080/15325008.2023.2237022.
19. Mishra S, Shaik AG. Solving bi-objective economic-emission load dispatch of diesel-wind-solar microgrid using African vulture optimization algorithm. Heliyon. 2024;10(3):e24993. doi:10.1016/j.heliyon.2024.e24993.
20. Ahmad Ahangar P, Ahmad Lone S, Gupta N. A data-driven-based optimal planning of renewable rich microgrid system. Arab J Sci Eng. 2024;49(5):6241–57. doi:10.1007/s13369-023-08153-5.
21. Guan J, Chen S, Xu H, Zhang Y. Distributed predefined-time economic dispatch algorithm for microgrid. J Frankl Inst. 2025;362(8):107672. doi:10.1016/j.jfranklin.2025.107672.
22. Candra OC. Energy management of smart microgrid considering hybrid optimal consumption of demand side. Oper Res Forum. 2025;6(2):50. doi:10.1007/s43069-025-00451-y.
23. Cagnano A. Can integrating SoC management in economic dispatch enhance real-time operation of a microgrid? Energies. 2025;18(7):1802. doi:10.3390/en18071802.
24. Dey B, Misra S, Sharma G, Bokoro PN. Cost-effective optimal scheduling of PHEV integrated microgrid with load curve restructuring strategies. Discov Comput. 2025;28(1):26. doi:10.1007/s10791-025-09521-5.
25. Ye X, Yang P. Economic optimal dispatch of networked hybrid renewable energy microgrid. Systems. 2025;13(2):109. doi:10.3390/systems13020109.
26. Zhang Y, Zhang Y, Liu Z, Chen Z. Gossip-based algorithm for economic dispatch of microgrids integrating isolated and grid-connected modes. Sci China Inf Sci. 2025;68(3):132204. doi:10.1007/s11432-024-4140-5.
27. Guo X, Gu F, Liu H, Yu Y, Li R, Wang J. Sustainable PV-hydrogen-storage microgrid energy management using a hierarchical economic model predictive control framework. Energy Inform. 2025;8(1):18. doi:10.1186/s42162-025-00482-z.
28. Liu T, Li Y, Qin X. Hybrid strategy improved Harris Hawks optimization algorithm for global optimization and microgrid economic scheduling problem. Clust Comput. 2025;28(3):177. doi:10.1007/s10586-024-04685-z.
29. Rollinson W, Urquhart A, Thomson M. Technoeconomic feasibility of wind and solar generation for off-grid hyperscale data centres. Energies. 2025;18(2):382. doi:10.3390/en18020382.
30. Mo D, Li Q, Sun Y, Zhuo Y, Deng F. Design of a new energy microgrid optimization scheduling algorithm based on improved grey relational theory. Algorithms. 2025;18(1):36. doi:10.3390/a18010036.
31. Zhu S, Wang E, Zeng F. Optimization control method for low-voltage DC microgrid with low carbon, economy, and reliability. ACS Omega. 2024;9(52):51665–78. doi:10.1021/acsomega.4c09671.
32. Khou SA, Olamaei J, Hosseini MH. Strategic scheduling of the electric vehicle-based microgrids under the enhanced particle swarm optimization algorithm. Sci Rep. 2024;14(1):30795. doi:10.1038/s41598-024-81049-y.